REPORT DOCUMENTATION PAGE

1

Form Approved OMB NO. 0704-0188

1. REPORT DATE (DD-MM-YYYY)	2. REPORT TYPE	3. DATES COVERED (From - To)
	New Reprint	-

4. TITLE AND SUBTITLE

Large Area and Depth-Profiling Dislocation Imaging and Strain Analysis in Si/SiGe/Si Heterostructures

5a. CONTRACT NUMBER

W911NF-10-1-0524

5b. GRANT NUMBER

5c. PROGRAM ELEMENT NUMBER

611103

6. AUTHORS

Xin Chen, Daniel Zuo, Seongwon Kim, James Mabon, Mauro Sardela, Jianguo Wen, Jian-Min Zuo

5d. PROJECT NUMBER

5e. TASK NUMBER

5f. WORK UNIT NUMBER

7. PERFORMING ORGANIZATION NAMES AND ADDRESSES

University of Illinois - Urbana
c/o OSPRA
1901 S. First Street, Suite A
Champaign, IL 61820 -7406

8. PERFORMING ORGANIZATION REPORT NUMBER

9. SPONSORING/MONITORING AGENCY NAME(S) AND ADDRESS (ES)

U.S. Army Research Office
P.O. Box 12211
Research Triangle Park, NC 27709-2211

10. SPONSOR/MONITOR'S ACRONYM(S)

ARO

11. SPONSOR/MONITOR'S REPORT NUMBER(S)

58141-EL-MUR.59

12. DISTRIBUTION AVAILIBILITY STATEMENT

Approved for public release; distribution is unlimited.

13. SUPPLEMENTARY NOTES

The views, opinions and/or findings contained in this report are those of the author(s) and should not contrued as an official Department of the Army position, policy or decision, unless so designated by other documentation.

14. ABSTRACT

We demonstrate the combined use of large area depth-profiling dislocation imaging and quantitative composition and strain measurement for a strained Si/SiGe/Si sample based on nondestructive techniques of electron beam-induced current (EBIC) and X-ray diffraction reciprocal space mapping (XRD RSM). Depth and improved spatial resolution is achieved for dislocation imaging in EBIC by using different electron beam energies at a low temperature of ~7 K. Images recorded clearly show dislocations distributed in three regions of the sample: deep dislocation networks concentrated in the "strained" SiGe region, shallow misfit dislocations at the top Si/SiGe

15. SUBJECT TERMS

electron beam-induced current (EBIC), transmission electron microscopy (TEM), X-ray diffractionelectron beam-induced current (EBIC), transmission electron microscopy (TEM), X-ray diffraction, reciprocal space mapping (XRD RSM), strained silicon,

16. SECURITY CLASSIFICATION OF:			17. LIMITATION OF ABSTRACT	15. NUMBER OF PAGES	19a. NAME OF RESPONSIBLE PERSON
a. REPORT	b. ABSTRACT	c. THIS PAGE			Daniel Wasserman
UU	UU	UU	UU		19b. TELEPHONE NUMBER 000-000-0000

Report Title

Large Area and Depth-Profiling Dislocation Imaging and Strain Analysis in Si/SiGe/Si Heterostructures

ABSTRACT

We demonstrate the combined use of large area depth-profiling dislocation imaging and quantitative composition and strain measurement for a strained Si/SiGe/Si sample based on nondestructive techniques of electron beam-induced current (EBIC) and X-ray diffraction reciprocal space mapping (XRD RSM). Depth and improved spatial resolution is achieved for dislocation imaging in EBIC by using different electron beam energies at a low temperature of ~7 K. Images recorded clearly show dislocations distributed in three regions of the sample: deep dislocation networks concentrated in the “strained” SiGe region, shallow misfit dislocations at the top Si/SiGe interface, and threading dislocations connecting the two regions. Dislocation densities at the top of the sample can be measured directly from the EBIC results. XRD RSM reveals separated peaks, allowing a quantitative measurement of composition and strain corresponding to different layers of different composition ratios. High-resolution scanning transmission electron microscopy cross-section analysis clearly shows the individual composition layers and the dislocation lines in the layers, which supports the EBIC and XRD RSM results.

REPORT DOCUMENTATION PAGE (SF298)
(Continuation Sheet)

Continuation for Block 13

ARO Report Number 58141.59-EL-MUR
Large Area and Depth-Profiling Dislocation Imag...

Block 13: Supplementary Note

Approved for public release; distribution is unlimited.

Microsc. Microanal., page 1 of 7
doi:10.1017/S1431927614012963

Microscopy AND Microanalysis

Large Area and Depth-Profiling Dislocation Imaging and Strain Analysis in Si/SiGe/Si Heterostructures

Xin Chen,[1,2,3] Daniel Zuo,[4] Seongwon Kim,[5] James Mabon,[2] Mauro Sardela,[2] Jianguo Wen,[2,6] and Jian-Min Zuo[1,2,*]

[1]*Department of Materials Science and Engineering, University of Illinois at Urbana-Champaign, Urbana, IL 61801, USA*
[2]*Frederick Seitz Materials Research Laboratory, University of Illinois at Urbana-Champaign, Urbana, IL 61801, USA*
[3]*Key Laboratory for Ultrafine Materials of Ministry of Education, Shanghai Key Laboratory of Advanced Polymeric Materials, School of Materials Science and Engineering, East China University of Science and Technology, Shanghai 200237, P. R. China*
[4]*Department of Electrical and Computer Engineering, University of Illinois at Urbana-Champaign, Urbana, IL 61801, USA*
[5]*Engineering Ceramic Center, Korea Institute of Ceramic Engineering and Technology, Icheon 467-843, Korea*
[6]*Argonne National Laboratory, Electron Microscopy Center, Nanoscience & Technology, Argonne, IL 60439, USA*

Abstract: We demonstrate the combined use of large area depth-profiling dislocation imaging and quantitative composition and strain measurement for a strained Si/SiGe/Si sample based on nondestructive techniques of electron beam-induced current (EBIC) and X-ray diffraction reciprocal space mapping (XRD RSM). Depth and improved spatial resolution is achieved for dislocation imaging in EBIC by using different electron beam energies at a low temperature of ~7 K. Images recorded clearly show dislocations distributed in three regions of the sample: deep dislocation networks concentrated in the "strained" SiGe region, shallow misfit dislocations at the top Si/SiGe interface, and threading dislocations connecting the two regions. Dislocation densities at the top of the sample can be measured directly from the EBIC results. XRD RSM reveals separated peaks, allowing a quantitative measurement of composition and strain corresponding to different layers of different composition ratios. High-resolution scanning transmission electron microscopy cross-section analysis clearly shows the individual composition layers and the dislocation lines in the layers, which supports the EBIC and XRD RSM results.

Key words: electron beam-induced current (EBIC), transmission electron microscopy (TEM), X-ray diffraction reciprocal space mapping (XRD RSM), strained silicon, dislocations

Introduction

Strained Si/SiGe/Si heterostructure is a technological material that offers the combined advantage of Si semiconductor technology and band gap engineering (Kittler et al., 1995). Inside the Si/SiGe/Si heterostructure, SiGe is compositionally graded and strain relaxed. The use of SiGe as a buffer allows for the fabrication of a wafer-scale strained Si layer by creating a larger in-plane lattice constant on a Si substrate. By optimizing the band structure of strained Si in a process called band engineering, mobility enhancement factors can be obtained over bulk Si with ~2 for electrons and as high as ~10 for holes. It thus provides a promising route toward high-speed Si devices (Mooney, 1996; Yuan et al., 2004; Chu et al., 2009), and an alternative to bulk silicon in the CMOS technology (Paul, 2004; Zhang et al., 2008). Strain relaxation via dislocations results in carrier scattering sites, which increases leakage current and degrades mobility. It also brings about undesirable strain reduction and surface roughness, which degrades the device performance (Yuan et al., 2004; Yuan et al., 2005; Zhang et al., 2008). Thus, the strain and dislocations in the Si/SiGe/Si heterostructure need to be carefully managed to reduce dislocations threading through the device layers at the top of the sample (Mooney, 1996; Yuan et al., 2005). This is mainly achieved by alternating compositions inside the heterostructure. Thus, characterization of dislocations, strains, and compositions are of critical importance for both device applications and materials synthesis (Kittler et al., 1995; Yuan et al., 2004).

Electron beam-induced current (EBIC) technology (Donolato, 1981) provides a powerful way for observing dislocation over relatively large areas of samples (Leamy, 1982; Higgs & Kittler, 1993; Yuan et al., 2004). It has the advantage of in-depth imaging of electronic active defects with a relatively good spatial resolution, although its signal/noise ratio needs to be carefully handled and its spatial resolution is limited by electron scattering and the carrier diffusion length. X-ray diffraction reciprocal space mapping (XRD RSM) is a quantitative strain analysis technique. The mapping is achieved by combining the ω and ω-2θ scan modes of XRD analysis, which can be used to determine lattice parameter change in the sample very accurately, and provide very useful strain and composition information (Yousif et al., 2001; Yamamoto et al., 2004; Ferrari & Bocchi, 2008; Shah et al., 2012). Transmission electron microscopy (TEM) offers excellent spatial resolution, and can be used to image individual dislocations in the sample in more detail (Yamamoto et al., 2004; Yuan et al., 2004). Composition analysis performed in a TEM system further allows determination of local composition. However, a major disadvantage of TEM analysis is the sample preparation, which

Received July 24, 2013; accepted July 17, 2014
*Corresponding author. jianzuo@illinois.edu

is destructive and time consuming. In addition, owing to the small sampling area, TEM is more suited for high-resolution analysis.

In this paper, we report a combined large area non-destructive analysis of a Si/SiGe/Si heterostructure using a combination of EBIC and XRD RSM. Using a combination of different electron beam energies and low sample temperature for EBIC, we are able to resolve both threading and misfit dislocations (MDs) at different sample depths. Dislocation characterizations of EBIC are correlated with TEM observations. Composition analysis is also performed based on the XRD RSM results and compared with scanning transmission electron microscopy (STEM)-based energy-dispersive spectroscopy (EDS) analysis. Comparison of these three techniques demonstrates that the combination of depth resolved EBIC imaging and XRD RSM allows for an extraction of complete information of composition, strain, and dislocations of the sample. The principles of our analysis are general. Further applications can have a significant impact on advancing semiconductor heterostructure research and development.

Experimental Methods

A Si/SiGe/Si (100) heterostructure sample provided by Texas Instrument (Dallas, Texas, USA) was used for the experiment. Inside the heterostructure, there is a three layer step graded (strained) region with a total thickness of 1.9 μm on top of the Si substrate, which is followed by a 2.65 μm uniform (relaxed) SiGe layer, and then a 17 nm strained silicon nano layer. For the EBIC experiment, a 700 Å thick aluminum thin film was deposited on the sample by e-beam evaporation to form a Schottky contact. A Temescal E-Beam Evaporation System (Livermore, California, USA) was used for the coating, with a background pressure of 10^{-6} Torr. The sample was cleaned with dilute HF solution (H_2O:HF = 10:1) for 30 s before the aluminum deposition. The top aluminum electrode and the silicon substrate were wired to a current collecting circuit through silver paste bonding. The EBIC measurement was performed in a Jeol 7000F Analytical SEM system (Jeol, Peabody, MA, USA). A low-noise current preamplifier (SR570; Stanford Research Systems Inc., Sunnyvale, CA, USA) was used to collect the EBIC signal from the sample, and to convert it to a voltage signal for imaging on the SEM. A liquid helium cooled sample stage was used for low temperature measurements. XRD RSM analysis was performed with a Philips X'pert MRD system (Philips, PANalytical, Almelo, the Netherlands). Si and SiGe [224] peaks were monitored for the RSM analysis. The cross-sectional TEM and EDS experiment was done on a Jeol JEM2010F (S)TEM system under the high-angle annular dark-field (HAADF) STEM mode using 200 keV electrons.

Results and Discussion

Depth-Profiling Dislocation Imaging Using EBIC

Figure 1 is an EBIC image of the sample obtained at 30 keV electron beam energy and at room temperature (RT),

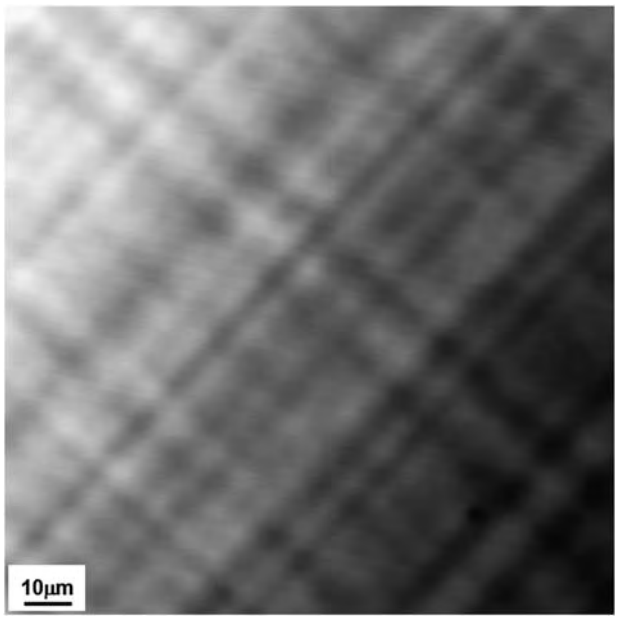

Figure 1. Electron beam-induced current image of the sample obtained at room temperature with 30 keV, 25 nA beam current.

showing the typical cross-hatch pattern (Yuan et al., 2004; Pizzini et al., 2006) that arises from MD networks deep in the sample. These MD lines are in the directions of [011] and [01-1] that are determined based on the sample edge orientation. In order to get a clear image with the low signal level at room temperature, we used a high-beam current of 25 nA. The image shows a brighter contrast on the left compared with the right side. This is caused by the voltage drop caused by the aluminum film resistance, with the left side being close to the current collecting pad.

We then cooled the sample temperature down to ~7 K using liquid helium and took EBIC images under different electron beam energies. The image at 30 keV shown in Figure 2a is similar to the RT one, but with the increased EBIC contrast at the lower temperature. In this case, we were able to get a clear image at 1 nA current. The image contrast also is highly uniform without the background brightness shift as seen at room temperature. Figure 2b is the low temperature EBIC taken at 20 keV electron beam energy. Besides the cross-hatched lines, dim dots appeared in the figure, showing threading dislocations (TDs) in the sample. In the EBIC image recorded at 3 keV electron beam energy (Fig. 2c), the cross-hatched lines seen from deep regions of the sample in Figure 2a disappeared, but thin lines corresponding to MDs at the top Si/SiGe interface region show up in the image, also black dots from TDs are seen in clear contrast.

Figure 2d is the EBIC image recorded at 3 keV EBIC as shown in high magnification, in which individual MDs and TDs are clearly seen. The dislocation densities can be measured directly from the figure. Such measurement gives an MD density at 5.1×10^3 cm^{-1} and the TD density at 9.6×10^6 cm^{-2}.

In Figures 3a and 3b we performed a comparison between the data recorded in Figures 2b and 2c. The dotted

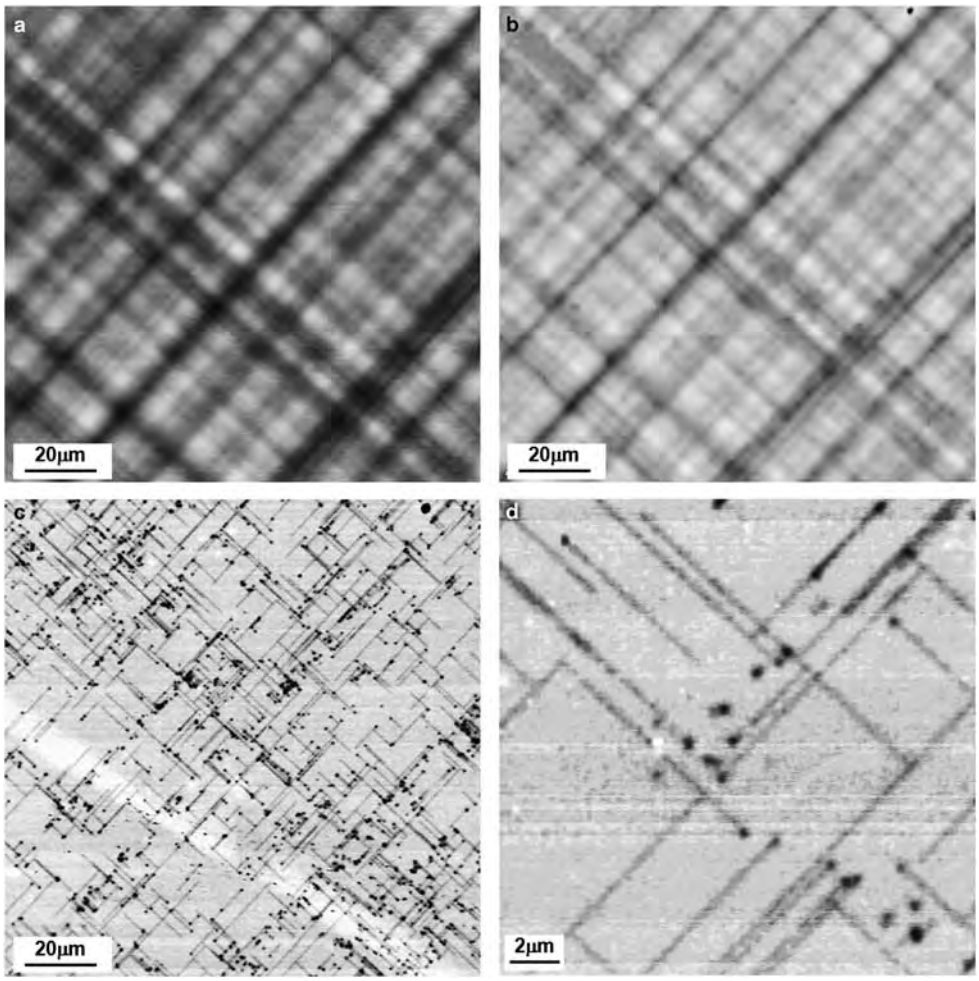

Figure 2. Electron beam-induced current images of the sample obtained at ~7 K, with 1 nA beam current at (**a**) 30 keV; (**b**) 20 keV; (**c**) 3 keV; and (**d**) 3 keV at larger magnification.

lines in Figure 3a mark the locations where the cross-hatched lines are strong in contrast, correlating to high-dislocation densities at those regions. These dotted lines are then superimposed on top of Figure 2c as shown in Figure 3b. This figure shows that the MD and TD densities seen from the top of the sample are high along the dotted lines, especially at the intersections of these lines, indicating a correlation between the top and bottom dislocations in the sample. Furthermore, the discernible dots from TD in Figure 3a are at almost the same locations as in Figure 3b, suggesting the TDs are possibly connecting the MDs at the top and the deep regions of the sample.

Figures 3c and 3d presents a simplified schematic illustration to explain the above results: a dislocation in the deep "strained" SiGe region bends up and penetrates through the "relaxed" SiGe layer and become a TD in the sample. Where the dislocation density is high in the "strained" SiGe regions as reflected by the stronger cross-hatched lines seen in EBIC, the possibility of generating a TD is also high. The TDs may directly penetrate the top strained Si layer as shown in Figure 3c, or it may glide (Mooney, 1996) at the strained Si and SiGe interface and form an MD line as shown in Figure 3d. In this way, the dislocations seen in the top sample region are correlated in position with those MDs in the deep sample region. As depicted in Figure 3d, at an end of an MD at the top Si and SiGe interface, the dislocation line connects to a TD into the deep region of the sample. The other possibility is that it may bend up and ends up at the top of the strained Si surface. When it connects to a TD into the sample, we see a dot at the end of the MD line in the low energy EBIC image. In the other case, the TD is too short to be seen in the EBIC image. The image of Figure 2d is consistent with this scenario. Some black dots are standing alone, suggesting the TDs have penetrated to the sample surface without forming MD lines at the top Si and SiGe interface. Other dots are located at the end of MD lines and some MDs end up with a black dot, while other ends do not. This observation is important as it provides detailed information about defect distributions at the top of the strained Si surface.

It is remarkable that the low temperature and electron beam energy significantly helps the contrast obtained in EBIC. The features identified by the EBIC contrast image correspond to defects where free carriers recombine, which

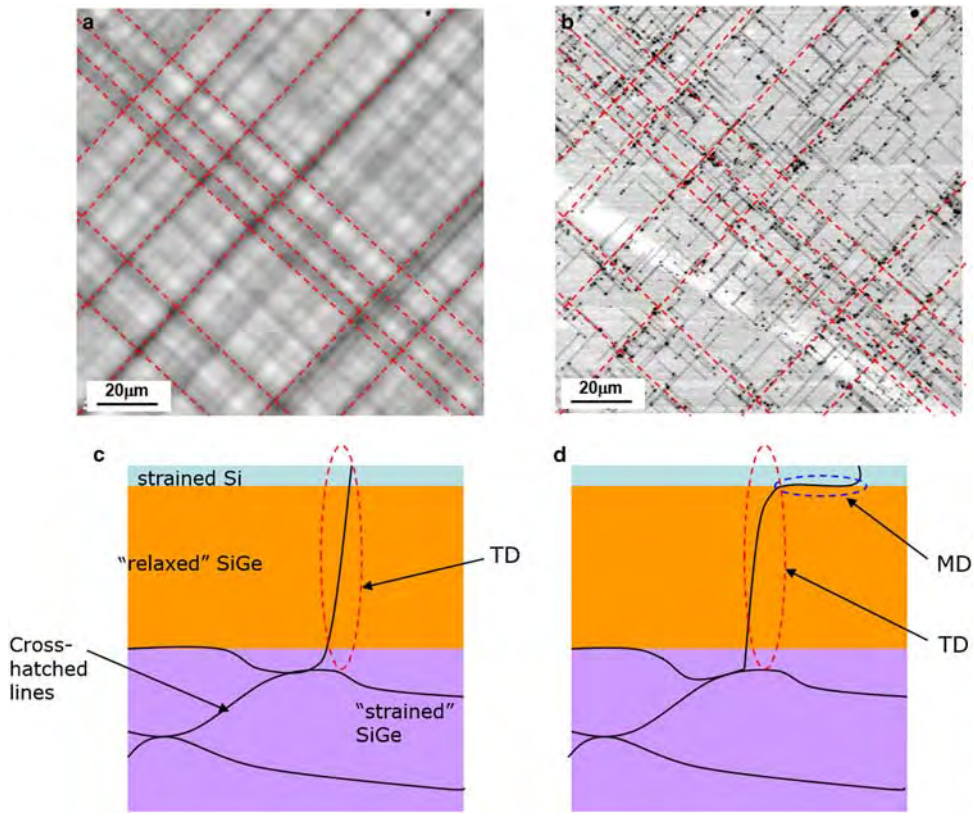

Figure 3. a, b: Compare electron beam-induced current images at different energies to see defect depth distributions in the sample. **c, d:** A schematic plot to show the correlations of the dislocations from different depths of the sample.

subtracts from the amplified current and causes a reduction in pixel value in the EBIC image. The contrast is increased by having either stronger recombination within the defect, or having a greater number of carriers reach the defect from the point of entry at the surface of the sample. The difference in contrast can mostly be attributed to the degree of overlap of the dislocation and the so-called "generation volume" created by the electron beam. As the generation volume expands in all three dimensions and the electron dose peak shifts to deeper regions of the sample as the beam energy increases, defects that are only imaged by a higher energy beam can thus be said to exist deeper within the sample.

To model this difference in visible depth, we simulated the distribution of electron energy density within the samples using a Monte Carlo simulation software package (CASINO, Drouin et al., 2007). A simulation was set up with a sample of identical material composition and layer depth as the experimental sample and simulated with an electron beam of 3, 5, 10, 20, and 30 keV beam energy and 1 nm beam size, and run for a total of 100,000 electrons. The resulting energy distribution data were integrated over the x and y dimensions and compared to show the depth dependence of the two energies. The data are shown in Figure 4a versus the depth in micrometers. The electron energy density simulation here clearly shows that electrons at 3 keV do not reach far beneath the surface and the overwhelming majority do not reach the "relaxed" SiGe/"Strained" SiGe boundary, whereas at 30 keV the electrons penetrate fully throughout the "relaxed" SiGe layer, "strained" SiGe layers, and even into the Si substrate at comparable energies to the SiGe layer. Thus, enough electron-hole pairs are generated in the "strained" SiGe layers for recombination that is owing to defects to show up in the contrast image obtained by EBIC.

The EBIC contrast (c) is proportional to the recombination strength of a dislocation to the first order approximation and energy density deposited by the electron beam. For the same energy density profile, assuming $c \sim 1/\tau$ with τ for the lifetime of the defect trapping state (Higgs & Kittler, 1994), the temperature dependence of c is determined by the temperature dependence of lifetime. Previous investigations have revealed two types of contrast temperature dependence for dislocations (Kittler et al., 1995), one increases with increasing temperature (type I) and the other increases with decreasing temperature (type II). What we see here with an increase in contrast at low temperature and the low signal level at RT are all consistent with the type II contrast. The type II contrast has been attributed to shallow trap levels. According to the Shockley–Hall–Reed model for shallow levels, the lifetime decreases upon cooling owing to Fermi level shifting toward the band edge. The shallow trap level is believed to be the intrinsic properties of dislocations.

The significant improvement in EBIC contrast at 3 keV can be attributed to the energy density profile. Figure 4b plots the energy deposited versus transverse distance from

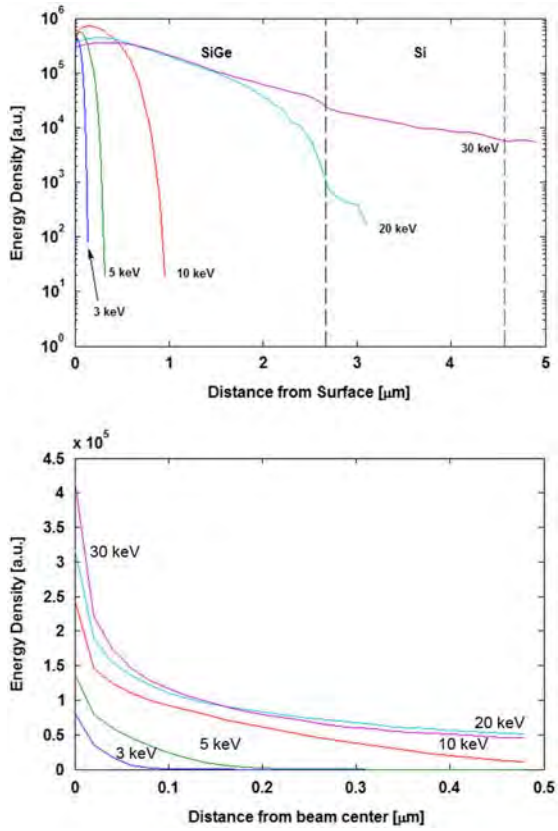

Figure 4. Top: Plot of electron energy density in arbitrary units versus depth, as simulated via Monte Carlo simulation. Five different electron beam energies were used: 3, 5, 10, 20, and 30 keV. Also shown are the major epitaxial layers in the sample: "relaxed" SiGe and "strained" SiGe, separated by dashed vertical lines. The Si substrate lies beneath the "strained" SiGe layers ($x \sim 5\,\mu m$). Bottom: Plot of electron energy density in arbitrary units versus transverse distance from the beam, as simulated via Monte Carlo simulation. A selection of different electron beam energies is used: 3, 5, 10, 20, and 30 keV (ascending in order of magnitude).

the electron beam obtained from the Monte Carlo simulations. At high-electron beam energies, the profile has a tail distribution that extends to several hundreds of nanometers. At 3 keV, the extent of energy density distribution has a half-width of 25 nm.

RSM

Figure 5 is the XRD RSM result recorded near the [224] diffraction node of the sample, which provides the following information about the sample. First, apart from the silicon substrate peak (marked as S), four distinct spots of $Si_{1-x}Ge_x$ (marked as L, 3, 4, and 5) are seen in Figure 5, indicating four distinctive layers of different composition ratios. The four peaks are broadened in the upper left to lower right direction, which result from lattice distortions that can be attributed to MDs in all the four layers. Among the four peaks, the three weaker peaks (3, 4, and 5) came from the thinner "strained" $Si_{1-x}Ge_x$ layers on the silicon substrate, and the strongest peak L has a composition ratio that correlates to the "relaxed" $Si_{1-x}Ge_x$ (18.6% Ge) layer on top of them. The strained Si peak 6 is directly above the "relaxed" 18.6% Ge one, suggesting the layer was almost fully strained with the $Si_{1-x}Ge_x$. The strained Si peak is broadened in the [001] direction, indicating the small thickness of the layer. Lattice parameter calculation shows the four $Si_{1-x}Ge_x$ layers are moderately strained with amplitudes varying from 0.05 to 0.12%, while the strained Si layer is strongly strained with $\varepsilon_\perp = -0.54\%$ and $\varepsilon_{//} = 0.90\%$. The long streaks pointing to the right in the figure are the analyzer streaks from the instrument.

Further results from the RSM analysis are listed in Table 1. The lattice parameters and the Ge concentrations of the different layers are calculated. The peak intensities roughly follow the layer thickness, with the strongest peak from the substrate and the weakest from the top strained silicon layer. Table 1 also lists the measured FWHMs. Compared with peak L, peaks 3–5 all have large FWHM, indicating the large amount of defects in their corresponding layers. Peak 5 height is relatively small partially owing to its larger FWHMs. For the strain Si, $a_{//}$ equals that of the SiGe layer L underneath it within the measurement precision, while EBIC results indicated an MD density of $5.1 \times 10^3\ cm^{-1}$.

Of further interest, as shown in Table 1, besides the silicon cap layer, all the SiGe layers also showed positive parallel strains ($Strain_{//}$'s). Silicon has a lattice parameter smaller than SiGe, thus, an epitaxial Si cap layer is supposed to have a positive $Strain_{//}$ owing to the lattice stretch from the SiGe layer underneath it. For the SiGe layers on the silicon substrate, the nonnegative $Strain_{//}$'s indicate there are other mechanisms determining the strains in them.

We note that the SiGe layers are deposited at elevated temperatures. At the high-growth temperatures, the strains might be relaxed owing to the production of dislocations, however, when the sample was cooled down, thermal expansion mismatch can cause new strains between the layers. The $Si_{1-x}Ge_x$ thermal expansion coefficients are larger than Si, with larger values for larger x (Schaffler, 2001), which we speculate as the cause of positive $Strain_{//}$s in the SiGe layers. In Table 1, we see $Si_{1-x}Ge_x$ layers with larger x values show relatively larger strains, correlating with their larger thermal expansion mismatch with the Si substrate. To compensate the lattice distortions as indicated by the positive $Strain_{//}$s, all the $Strain_\perp$s of the Si and SiGe layers showed negative values.

TEM Analysis

Figure 6a is the TEM cross-section image of the SiGe sample recorded in STEM using a HAADF detector. Different layers in the sample can be distinguished by the layer brightness, and the dislocations lines at the layer boundaries. The darkest part to the right is the silicon substrate, with the lower electron diffraction intensity resulting from the lower average atomic number. Above the substrate, there are three "strained" SiGe layers separated by the MD lines at the layer boundaries. Further to the left is the "relaxed" SiGe layer.

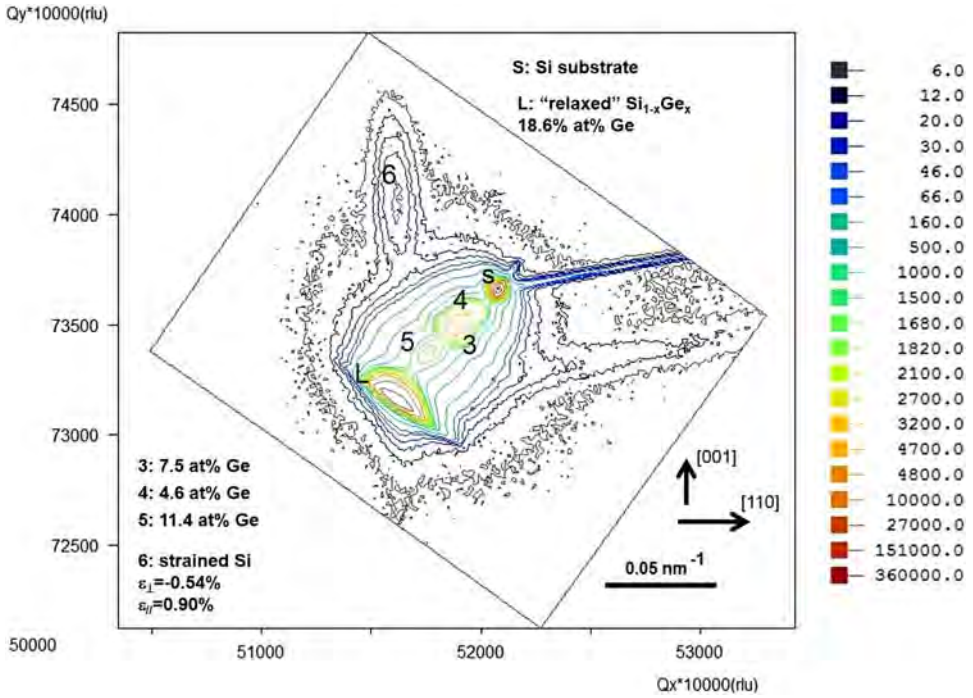

Figure 5. X-ray diffraction reciprocal space mapping on the Si/SiGe/Si heterostructural sample, monitoring Si and Ge [224] peaks.

Above the "relaxed" SiGe layer, is the very thin strained Si top layer, which is not discernible under this magnification. Besides the dislocations in the "strained" SiGe layers, there are also some dark lines in the "relaxed" SiGe region, confirming the existence of dislocation lines even in the "relaxed" SiGe layer of the sample.

Figure 5b shows the composition analysis on the sample. The squares are the EDS results on different locations of the sample, which clearly show the Ge concentration changes in the different layers of the sample. The triangles are the XRD RSM results plotted into the figure for comparison. The results from the two methods agree very well except the result for peak L in Figure 5.

Summary

In this paper, we reported nondestructive defect characterization in the Si/SiGe strained structures using depth-profiling EBIC and XRD RSM and by comparing with STEM analysis. Dramatically clear EBIC images were obtained by cooling the sample down to ~7 K. TDs and MDs near the top of the Si/SiGe structures are clearly imaged with the low temperature EBIC measurement and low kV electrons. XRD RSM analysis showed four composition regions of SiGe layers and gave accurate composition ratios in the layers; it also provides an accurate measurement of strain. The Si cap layer showed positive $Strain_{//}$ and negative $Strain_{\perp}$ owing to lattice parameter mismatch with the underlying layer; the four SiGe layers also showed positive $Strain_{//}$s and negative $Strain_{\perp}$s, which are attributed to thermal expansion mismatch with the silicon substrate. Both EBIC and X-ray RSM results are supported by TEM/EDS analysis. The study here demonstrates the complementary advantage of each technique employed here.

Acknowledgments

This work was carried out as part of the effort to establish the EBIC technique for semiconductor defect analysis at the

Table 1. The [224] Node XRD RSM Analysis Result on the Si/SiGe/Si Sample.

Peak #	Intensity	$a_{//}$ (nm)	$a_{\perp}$ (nm)	*x* Ge	FWHM*x*	FWHM*y*	$Strain_{//}$	$Strain_{\perp}$
S	3.84E + 05				2.05E-04	2.35E-04		
L	6.20E + 04	0.5480	0.5468	18.6%	4.69E-04	3.39E-04	0.12%	− 0.09%
3	3.50E + 03	0.5452	0.5444	7.5%	1.33E-03	1.44E-03	0.08%	− 0.06%
4	2.74E + 03	0.5445	0.5439	4.6%	1.92E-03	1.76E-03	0.06%	− 0.05%
5	1.85E + 03	0.5464	0.5452	11.4%	2.67E-03	2.46E-03	0.12%	− 0.10%
6	4.57E + 01	0.5480	0.5402		1.20E-03	1.06E-02	0.90%	− 0.54%

XRD RSM, X-ray diffraction reciprocal space mapping; FWHM, full-width at half-maximum.

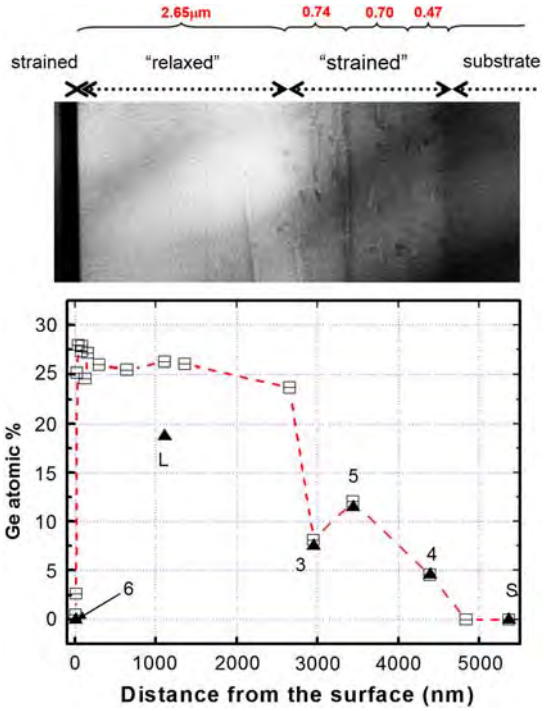

Figure 6. a: High-angle annular dark-field transmission electron microscopic (TEM) image showing individual layers and dislocation distributions in the sample. **b:** Energy-dispersive spectroscopy composition profile (square) in comparison with the X-ray diffraction reciprocal space mapping data (triangle). **c:** TEM image showing glided threading dislocation (TD) and TD toward the surface of the sample.

University of Illinois supported by the US Army Research Office (Grant No. Army W911NF-10-1-0524 and monitored by Dr. William Clark) through the MURI program. Dr. Chen is also supported by the Shanghai Leading Academic Discipline Project (B502), Shanghai Key Laboratory Project (08DZ2230500), and Science and Technology Commission of Shanghai Municipality Project (11nm0507000).

References

Chu, M., Sun, Y.K., Aghoram, U. & Thompson, S.E. (2009). Strain: A solution for higher carrier mobility in nanoscale MOSFETs. *Ann Rev Mater Res* **39**, 203–229.

Donolato, C. (1981). An analytical model of SEM and STEM charge collection images of dislocations in thin semiconductor layers. 2. EBIC images of dislocations. *Phys Status Solidi (a)* **66**(2), 445–454.

Drouin, D., Couture, A.R., Joly, D., Tastet, X., Aimez, V. & Gauvin, R. (2007). CASINO V2.42 – A Fast and Easy-to-use Modeling Tool for Scanning Electron Microscopy and Microanalysis Users. *Scanning* **29**, 92–101.

Ferrari, C. & Bocchi, C. (2008). Strain and composition determination in semiconducting heterostructures by high-resolution X-ray diffraction. In *Characterization of Semiconductor Heterostructures and Nanostructures*, Lamberti C. (Ed.), pp. 93–132. Amsterdam, the Netherlands: Elsevier B.V.

Higgs, V. & Kittler, M. (1993). Investigation of the recombination activity of misfit dislocations in Si/SiGe epilayers by cathodoluminescence imaging and the electron-beam-induced current technique. *Appl Phys Lett* **63**(15), 2085–2087.

Higgs, V. & Kittler, M. (1994). Influence of hydrogen on the electrical and optical activity of misfit dislocations in Si/SiGe epilayers. *App Phys Lett* **65**(22), 2804–2806.

Kittler, M., Ulhaqbouillet, C. & Higgs, V. (1995). Influence of copper contamination on recombination activity of misfit dislocations in SiGe/Si epilayers – Temperature-dependence of activity as a marker characterizing the contamination level. *J Appl Phys* **78**(7), 4573–4583.

Leamy, H.J. (1982). Charge collection scanning electron-microscopy. *J Appl Phys* **53**(6), R51–R80.

Mooney, P.M. (1996). Strain relaxation and dislocations in SiGe/Si structures. *Mater Sci Eng R* **17**(3), 105–146.

Paul, D.J. (2004). Si/SiGe heterostructures: From material and physics to devices and circuits. *Semicond Sci Technol* **19**(10), R75–R108.

Pizzini, S., Acciarri, M., Binetti, S., Ledonne, A., Marchionna, S. & Bollani, M. (2006). Defect studies on silicon and silicon-germanium for PV and optoelectronic applications. *Mater Sci Semicond Process* **9**(1–3), 66–73.

Schaffler, F. (2001). Silicon-Germanium (Si1-xGex). In *Properties of Advanced Semiconductor Materials GaN, AlN, InN, BN, SiC, SiGe*, Levinshtein M.E., Rumyantsev S.L. & Shur M.S. (Eds.), pp. 149–188. New York: John Wiley & Sons, Inc.

Shah, V.A., Dobbie, A., Myronov, M. & Leadley, D.R. (2012). Reverse graded strain relaxed SiGe buffers for CMOS and optoelectronic integration. *Thin Solid Films* **520**, 3227–3231.

Yamamoto, T., Sakai, A., Egawa, T., Taoka, N., Nakatsuka, O., Zaima, S. & Yasuda, Y. (2004). Dislocation structures and strain-relaxation in SiGe buffer layers on Si(001) substrates with an ultra-thin Ge interlayer. *Appl Surf Sci* **224**(1–4), 108–112.

Yousif, M.Y.A., Nur, O., Willander, M., Patel, C.J., Hernandez, C., Campidelli, Y., Bensahel, D. & Kyutt, R.N. (2001). Direct assessment of relaxation and defect propagation in different as-grown and in situ post-growth annealed thin Ge/Si and step-graded $Si_{1-x}Gex$/Si buffer layers. *Solid State Electron* **45**(11), 1869–1874.

Yuan, X.L., Sekiguchi, T., Niitsuma, J., Sakuma, Y., Ito, S. & Ri, S.G. (2005). Inhomogeneous distribution of dislocations in a SiGe graded layer and its influence on surface morphology and misfit dislocations at the interface of strained Si/Si0.8Ge0.2. *Appl Phys Lett* **86**(16), 162102-1 to 162102-3.

Yuan, X.L., Sekiguchi, T., Ri, S.G. & Ito, S. (2004). Study of dislocations in strained-Si/Si0.8Ge0.2 heterostructures by EBIC, TEM and etching techniques. *Eur Phys J-Appl Phys* **27**(1–3), 337–340.

Zhang, R.H., Rozgonyi, G.A., Yakimov, E., Yarykin, N. & Seacrist, M. (2008). Impact of thermal annealing on deep-level defects in strained-Si/SiGe heterostructure. *J Appl Phys* **103**(10), 103506-1 to 103506-7.